Journal of Adhesion Science and Technology

ISSN: 0169-4243 (Print) 1568-5616 (Online) Journal homepage: https://www.tandfonline.com/loi/tast20

# Injection-molded plastic plate with hydrophobic surface by nanoperiodic structure applied in uniaxial direction

Masaki Yamaguchi, Shinya Sasaki, Shojiro Suzuki & Yuki Nakayama

**To cite this article:** Masaki Yamaguchi, Shinya Sasaki, Shojiro Suzuki & Yuki Nakayama (2015) Injection-molded plastic plate with hydrophobic surface by nanoperiodic structure applied in uniaxial direction, Journal of Adhesion Science and Technology, 29:1, 24-35, DOI: 10.1080/01694243.2014.973158

**To link to this article:** https://doi.org/10.1080/01694243.2014.973158

*Journal of Adhesion Science and Technology*, 2015
Vol. 29, No. 1, 24–35, http://dx.doi.org/10.1080/01694243.2014.973158

# Injection-molded plastic plate with hydrophobic surface by nanoperiodic structure applied in uniaxial direction

Masaki Yamaguchi*, Shinya Sasaki, Shojiro Suzuki and Yuki Nakayama

*Biomedical Engineering & Robotics Laboratory, Graduate School of Engineering, Iwate University, 4-3-5 Ueda, Morioka 020-8551, Japan*

(*Received 23 June 2014; final version received 29 September 2014; accepted 30 September 2014*)

The purpose of this research is to establish a processing method for a wide-area nanometer scale periodic structure on the surface of a plastic plate in order to improve its hydrophobicity. We also evaluated the effect of a nanoperiodic structure applied in the uniaxial direction. Plastic plates of acrylonitrile–ethylene–styrene with dimensions of 100 × 100 $mm^2$ with a nanoperiodic structure on their surfaces were fabricated using a femtosecond laser and an injection molding technique. In the injection molding, the maximum transfer ratio for the depth reached as high as 0.79. When the nanoperiodic structure was applied in the uniaxial direction, the apparent contact angles did not decrease with respect to the direction of the ridges. As a result, the apparent contact angle increased by 20.4°, from 77.2° to 97.6° which is equivalent to 26%. In the six-month duration test, the sliding angle was initially decreased by applying the nanoperiodic structure. Additionally, the sliding angle was maintained between 20° and 38.3° during the duration test, which was lower than the angle for the flat plate at 42.7°. It can be considered that the depth was sufficient to maintain the sliding angle. In this condition, the contact angle hysteresis did not differ with or without the nanoperiodic structure on the surfaces, an effect that could be caused by surface dirt. In summary, the plastic plate was well drained and the characteristics were maintained for several months by forming the nanoperiodic structure on the surface.

**Keywords:** periodic structure; hydrophobic surface; femtosecond laser; injection molding; plastic plate; nanometer scale

## 1. Introduction

In many fields of technology, numerous studies into surface science have expanded our understanding of the repellency of liquid drops on a surface.[1] One of the ways of controlling the wettability of a solid surface is to increase the surface roughness. Investigations have been conducted that attempt to improve the physical wettability of solid surfaces by the addition of a periodic structure.[2] The lotus is a symbol of an extreme hydrophobic surface characterized by a high contact angle.[3] Superhydrophobic surfaces with a high contact angle above 150° exhibit extreme water repellence and self-cleaning properties.[4] Gao and colleagues reported on the progress of surface roughness-induced wettability throughout history.[5]

Surface roughness-induced wettability is prevalent in nature, and similar physical performance has started to switch from ‘natural’ design to industrial design. In order to

*Corresponding author. Email: masakiy@iwate-u.ac.jp

improve the performance of surfaces, such as their self-cleaning properties,[6] periodic structures have been applied to industrial products.[7] Previously, there have been some reports of methods that chemically modify molecules on the surface.[8,9] In particular, it seems that one effective approach to modifying surface roughness-induced wettability can be achieved by injection molding of plastic resins, because the wettability of the surface of a plastic product can be controlled by the addition of a periodic structure on the surface of a mold. To address the problem of surface processing for such a structure, some investigators have tried to form a periodic structure on moldings using a 'cutting' approach.[10] However, in cutting work, the scale of the processing is limited to the micrometer range by the size of the cutting device.

Birnbaum discovered in 1965 that a periodic structure on the scale of the laser wavelength was created by damage on the bottom of the processing marks of lasers.[11] Since then, laser-induced periodic grating structures have been reported by several researchers.[12] It is currently thought that a standing wave induced by interference between incident light and the plasma [13] or dispersion waves [14] is the origin of this periodic structure. This technique has already been tried to form periodic structures.[15,16] However, the injection molding conditions are not considered to be appropriate for the nanometer scale. As a result, it is not technically easy to form a nanometer scale periodic structure over an area wider than $100 \times 100\ mm^2$ during a realistic machining time.

The purpose of this study is to establish a processing method for a wide-area nanoperiodic structure on a plastic plate with dimensions of $100 \times 100\ mm^2$ using a femtosecond laser and injection molding in order to improve the hydrophobicity. To begin with, the characteristics of the nanoperiodic structures that were transferred to the plastic plates were compared with respect to the molding conditions. Subsequently, the hydrophobic properties of nanoperiodic structures applied in the uniaxial direction were investigated on the transferred surfaces of the plastic plates by studying circularity tolerance and apparent contact angle. Finally, we evaluated the hydrophobicity of the nanoperiodic structure by carrying out exterior environmental exposure duration tests and by monitoring sliding angle and contact angle hysteresis (CAH).

## 2. Materials and methods

### *2.1. Materials*

A steel mold (SKD11, annealed, 58.0 HRC of hardness, Hitachi Metals Tool Steel, Ltd., Japan) was used to produce a plastic plate with a nanoperiodic structure on the surface. Acrylonitrile–ethylene–styrene (AES; SK10, UMG ABS Ltd., Japan) was used to fabricate the plastic plate test pieces. The properties of the AES were as follows; milk white in color; $28\ cm^3/10$ min. of melt volume flow rate (220 °C, ISO 1133) [17]; 83 MPa of bending strength (ISO 178) [18]; and 53 MPa of tensile yield stress (ISO 527).[19] The (Young) equilibrium contact angle, $\theta$, for AES was estimated at 77.2° by observable contact angle [20] using distilled water, an AES flat plate fabricated by injection molding (25 nm of surface roughness), and a commercial contact angle analyzer (DM-701, Kyowa Interface Science Co. Ltd., Japan).

### *2.2. Manufacturing of mold with periodic structure*

The principle of a laser-induced periodic structure is shown in Figure 1. The surface of the metal is irradiated with a femtosecond laser with a pulse width shorter than the

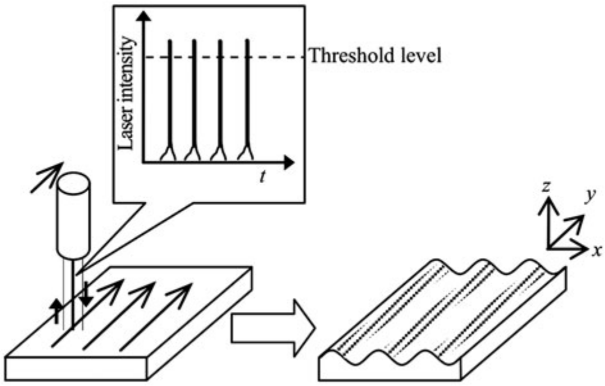


Figure 1. Principle of a laser induced nanoperiodic structure using a femtosecond laser (IFRIT-D, Cyber Laser Inc., Japan).

thermal relaxation time of the solid. A surface plasma wave is excited on the metal surface. Ion discharge takes place alternately in the areas where the energy intensity of the laser exceeds a threshold level. Ablation occurs on the metal surface and a periodic structure is formed on it.

The manufacturing process of a metal mold with a nanoperiodic structure applied to it in a uniaxial direction was accomplished through the following steps:

(1) As a pre-processing step, the base material is polished by hand to achieve a surface roughness, $R_a$, of 0.05 μm with dimensions of 100 × 100 $mm^2$.
(2) A femtosecond laser (Ti-sapphire laser, IFRIT, Cyber Laser Inc., Japan) is used to induce a periodic structure. The wavelength, pulse width, output power, and scanning speed of the femtosecond laser are 780 nm, 210 fs, 261.4 mW and 1.5 mm/s, respectively. When the scanning is carried out in the *y*-direction over a length of 100 mm, several mm width of periodic structure will be processed simultaneously in the *x*-direction (Thus, the uniaxial direction of the periodic structure is processed in the *x*-direction). Then the residual processing powder is removed using $N_2$ gas.
(3) Scanning in the *y*-direction is repeated several times until a 100-mm width of the periodic structure is fabricated in the *x*-direction.

### *2.3. Injection molding of test pieces*

Test pieces of AES were fabricated using an injection molding machine (Si-100II, Toyo Machinery & Metal Ltd., Japan) with a filling pressure of 14.7 kN, a filling time of 30 s, and a mold temperature of 50 °C, respectively. Four kinds of molding conditions were examined in this study by changing the holding pressure and the dwelling time which include: type A: 6.9 kN of holding pressure and 5 s of dwelling time; type B: 7.5 kN of holding pressure and 5 s of dwelling time; type C: 7.5 kN of holding pressure and 10 s of dwelling time; and type D: 6.9 kN of holding pressure and 10 s of dwelling time.

The surface textures of both the metal mold and the test pieces were examined in terms of the pitch, $\tau$, the depth, $d$, the surface roughness, and the surface waviness using a non-contact laser confocal microscope (1 nm of resolution for depth, OLS4100, Olympus Co., Japan). The surface roughness and the surface waviness were calculated as arithmetic averages, $R_a$, and $W_a$, respectively. Additionally, the depth was measured five times for each condition and the mean value was recorded. Finally, the transfer ratio of the depth, $\delta = d/d_m$, was calculated for each test piece (where, $d_m$ is the depth of the metal mold). The surface texture was measured both at the center and at the edge.

### 2.4. Circularity tolerance and apparent contact angle

The hydrophobic properties of nanoperiodic structures applied in the uniaxial direction were investigated on the transferred surfaces of the plastic plates by monitoring circularity tolerance and apparent contact angle.

Prior to evaluating the wettability, the test pieces were ultrasonically cleaned in distilled water for 10 min, and dried for several seconds using $N_2$ gas. Immediately after that, the test pieces were diselectrified with an ionizer (SJ-M400, Keyence Co., Japan) and the surface potentials were confirmed using a surface electrometer (SK-025/200, Keyence Co., Japan) at less than −15 V.

A microscope (VH-E500, Keyence Co., Japan) and image analysis software (half-angle method, Image J, Open source) were used to measure the apparent contact angles, $\theta'$, of the nanoperiodic structures. The amount of water dropped onto the surface was set to 1 μL using a microsyringe with distilled water in order to decrease the influence of gravity. The measurements were repeated three times using different areas.

### 2.5. Duration test, sliding angle, and CAH

An exterior environmental exposure duration test was carried out for the test pieces fabricated using type B conditions. The rooftop of the four-story building of Iwate University in Morioka, Japan, was selected as the experimental location and the test duration continued over a six-month period. The plastic plates were set on a table inclined at 30° to the horizon, which is equivalent to the setting angle of a solar battery. Three different test pieces were set on the table; a test piece with a periodic structure set along the direction of gravity (i.e. the vertical direction), a test piece with a periodic structure set in the direction horizontal to gravity (horizontal direction), and a test piece without a periodic structure (flat plate). The temperature, $T$, the relative humidity, RH, the integrated precipitation, $R$, and the integrated intensity of the ultraviolet radiation, UV, were continuously monitored as the environmental indexes. The color difference, $\Delta E^*_{ab}$, the depth, the characteristics of hydrophobicity,[21] sliding angle (the surface tilt required to achieve motion). and the CAH (the difference between the advancing angle, $\theta_A$, and the receding angle, $\theta_R$; CAH = $\theta_A - \theta_R$) were continuously monitored as the hydrophobic indexes.

The most common techniques of measuring CAH are the sessile drop and the Wilhelmy plate technique.[22] In order to evaluate a condition similar to the industrial application such as a solar battery, both the sliding angle and the CAH were measured by the tilted plate method [23] using the commercial contact angle analyzer. In a preliminary step, the sliding angle was found to depend on the volume of the droplet.[24] Therefore, the volume of the water drops was set at 30 μL to simulate raindrops. Each water drop was first deposited on a horizontal substrate and when equilibrium was reached, the substrate was tilted at a rate of 120°/min until the onset of drop motion. The measurements were repeated three times using different areas.

### 2.6. Statistical analysis

All analyses were performed using the Statistical Package for the Social Sciences (SPSS) version 20.0 (SPSS Inc., Chicago, IL). Unless stated otherwise, all of the data are expressed as the mean ± standard deviation (SD).

## 3. Results

### 3.1. Manufacturing of periodic structure

Figure 2 shows an external view of a metal mold with a laser-induced nanoperiodic structure applied in the uniaxial direction. A periodic structure with a 780 ± 26 nm pitch was formed on the surfaces, which is in good agreement with the wavelength of the femtosecond laser. The depths were 372 ± 19 nm at the center and 342 ± 32 nm on the corner edge. The nanoperiodic structure was formed in a self-organized way by the femtosecond laser, and the width of the nanoperiodic structure in each *y*-direction scan was 2 mm. Thus, 50 scan were needed to form a 100-mm width nanoperiodic structure, and no disturbances were observed at the joints between the different scans. Under the condition where a scanning speed of 1.5 mm/s was used, <1 h of machining time was needed to form a nanoperiodic structure with dimensions of 100 × 100 mm$^2$.

### 3.2. Injection molding of test pieces

The surface roughness, $R_a$, ranged between 14 and 23 nm at both the center and the corner edge (Table 1) whereas $R_a$ of the flat plate was 23 nm. Also, the surface waviness, $W_a$, ranged between 21 and 46 nm, whereas $W_a$ of the flat plate was 29 nm. The depth, $d$, showed a maximum value for the type B condition, both at the center and at the corner edge, and the values were 295 ± 79 and 271 ± 69 nm, respectively. As a result, the transfer ratio for the depth had a distribution from 0.41 to 0.79. Thus, the surface textures of the nanoperiodic structure showed maximum values for the type B condition, and the transfer ratio for the depth reached as high as $\delta = 0.79$.

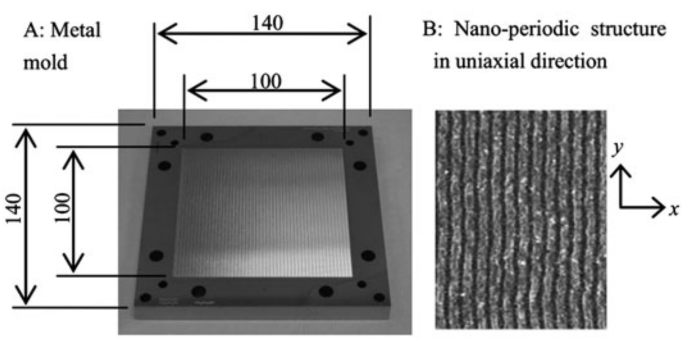


Figure 2. External view of a mold with a laser-induced nanoperiodic structure (units in mm).

Table 1. Surface roughness and surface waviness of the four types of test pieces with nanoperiodic structure (nm).

| | Surface roughness, $R_a$ | Surface waviness, $W_a$ | Depth*, $d$ | Transfer ratio, $\delta$ |
|---|---|---|---|---|
| Center | | | | |
| A | 9 | 21 | 154 ± 29 | 0.41 |
| B | 23 | 29 | 295 ± 79 | 0.79 |
| C | 14 | 32 | 205 ± 39 | 0.55 |
| D | 16 | 30 | 219 ± 46 | 0.59 |
| Corner edge | | | | |
| A | 14 | 25 | 196 ± 31 | 0.57 |
| B | 23 | 46 | 271 ± 69 | 0.79 |
| C | 16 | 31 | 230 ± 27 | 0.67 |
| D | 17 | 40 | 223 ± 28 | 0.65 |

*$n$ = 5.

### 3.3. *Circularity tolerance and apparent contact angle*

The circularity tolerances of the flat plate and the test piece with a nanoperiodic structure (type B) were 0.92 ± 0.03 and 0.87 ± 0.02, respectively (Table 2). In the test piece with the nanoperiodic structure (type B), the apparent contact angles observed from the $x$-direction and $y$-directions were 97.6° ± 0.86° and 96.4° ± 2.42°, and the difference between them was 1.2%. The type B condition exhibited the maximum apparent contact angle (Table 3). The apparent contact angle increased by 20.4°, from 77.2° to 97.6°, which is equivalent to a 26% improvement compared with the original value.

Table 2. Circularity and difference of the apparent contact angle of the $x$- and $y$-directions of type B test piece.

| | Flat plate | Type B test piece with nanoperiodic structure | |
|---|---|---|---|
| Circularity tolerance (top view) | 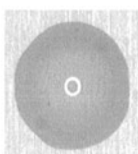 0.92 ± 0.03 | 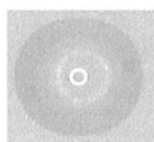 0.87 ± 0.02 | |
| Apparent contact angle (side view) |  *77.2 ± 0.68° | Observed from $y$-direction 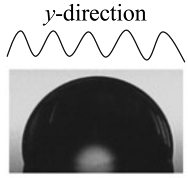 97.6 ± 0.86° | Observed from $x$-direction 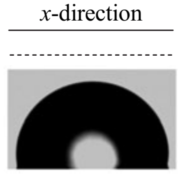 96.4 ± 2.42° |

*Equilibrium contact angle, $\theta$.

Table 3. The apparent contact angles, $\theta'$, on the test pieces observed from the $y$-direction.

| Type | *Flat plate | Test piece with nanoperiodic structure (increased value) |
|---|---|---|
| A | 77.2° | 78.0° (+0.8°) |
| B | | 97.6° (+20.4°) |
| C | | 94.9° (+17.7°) |
| D | | 89.8° (+12.6°) |

*Equilibrium contact angle, $\theta$.

### 3.4. Duration test, sliding angle, and CAH

The exterior environmental exposure duration test was carried out from 1 June to 30 November 2013, which included the Summer, Autumn, and Winter seasons. During the experimental period, the mean temperature and mean RH were 20 °C and 77%, respectively (Figure 3). The integrated precipitation, $R$, and the intensity of the ultraviolet radiation, UV, were 1228 mm and 47 mW/cm$^2$, respectively. The color difference, $\Delta E^*_{ab}$, of the test piece increased from 2.4 to 10.5 during the experiment.

After the six-month duration test, the depths of the type B test pieces for the horizontal and vertical directions decreased from 295 ± 79 to 175 ± 47 nm (−41%) and from 295 ± 79 to 181 ± 28 nm (−39%), respectively (Table 4). No regularity was observed in the surface roughness of the test pieces with time, and the values were similar to those of the flat plate at 23 nm.

The initial values of sliding angle on the flat plate, on the test piece with the periodic structure in the vertical direction, and the test piece with the periodic structure in the horizontal direction were 42.7°, 34.0° and 37.7°, respectively (Figure 4). In the six-month duration test, the sliding angle of the test pieces with the periodic structure in the vertical direction distributed between 20° and 38.3° during the duration test which were lower angles than that of flat plate at 42.7°. This tendency was similar to the test piece with the periodic structure in the horizontal direction, when the sliding angle distributed between 19.7° and 32.0°.

The differences in the values for the cosine for the receding and advancing angles, $\cos\theta_R - \cos\theta_A$, were calculated. The initial values of ($\cos\theta_R - \cos\theta_A$) on the flat plate, on the test piece with the periodic structure in the vertical direction, and the test piece with the periodic structure in the horizontal direction were 0.46, 0.47, and 0.55, respectively. The values of ($\cos\theta_R - \cos\theta_A$) for the test pieces with periodic structure in the vertical direction distributed between 0.36 and .059 during the duration test. This tendency was similar to the case of the test piece with the periodic structure in the horizontal-direction, when the values of ($\cos\theta_R - \cos\theta_A$) were distributed between 0.25 and 0.55. There was no difference between the CAH with and without the presence of a nanoperiodic structure.

The initial values of CAH on the flat plate, on the test piece with the periodic structure in the vertical direction, and on the test piece with the periodic structure in the horizontal direction were 26.8°, 27.5° and 31.9°, respectively. In the six-month duration test, the CAH of the test piece with the periodic structure in the vertical direction distributed between 21.4 and 35.5° during the duration test. This tendency was similar to the case of the test piece with the periodic structure in the horizontal direction, when the CAH was distributed between 19.5° and 28.2°. There was no difference between the CAH with and without the presence of a nanoperiodic structure.

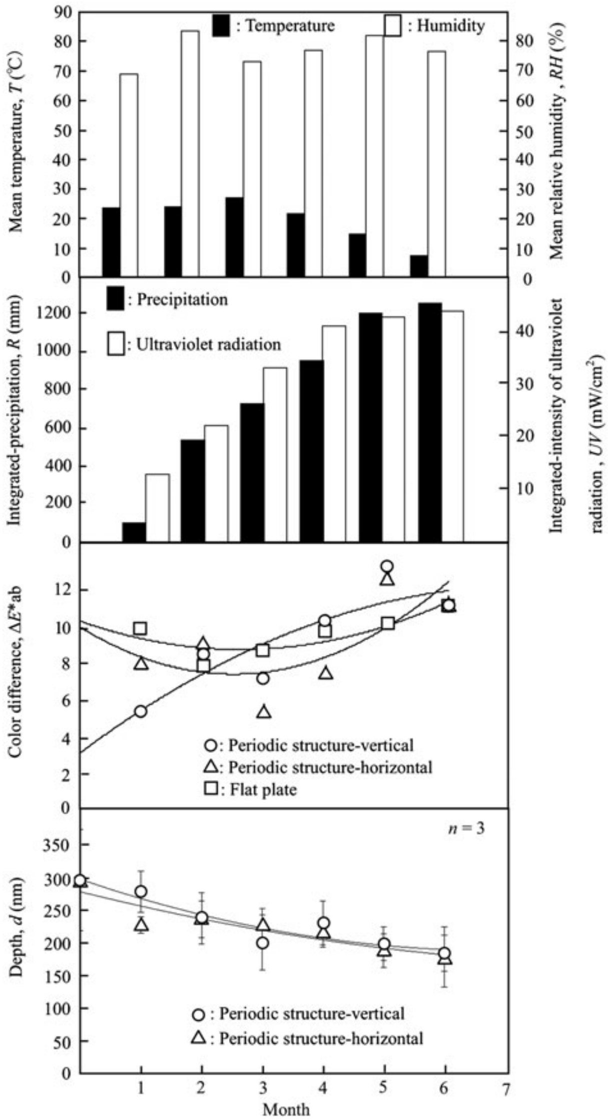


Figure 3. Time-course changes of the environmental indexes in an exterior environmental exposure duration test for 6 months (error bar: SD).

## 4. Discussion

A laser-induced nanoperiodic structure with dimensions of $100 \times 100\ \text{mm}^2$ could be formed at 780-nm pitch and 372-nm depth within 1 h of machining time. The nanoperiodic structure consisted of 128,200 lines/100 mm.

In the injection molding of test pieces, the maximum transfer ratio for the depth reached as high as 0.79. It was revealed that a holding pressure of 7.5 kN was needed and a dwelling time of 5 s (type B condition) was sufficient. It is believed that the transfer ratio depends on the melt volume flow rate and the temperature of the resin. It was found that the type B condition exhibited the maximum apparent contact angle,

Table 4. Time-course changes of the surface roughness and the depth of type B test pieces in the duration test for six-month period (units in nm).

| Duration (month) | | Surface roughness, $R_a$ | Depth*, $d$ |
|---|---|---|---|
| 0 (center) | | 23 | 295 ± 79 |
| Vertical-direction | 1 | 25 | 277 ± 32 |
| | 2 | 20 | 236 ± 40 |
| | 3 | 18 | 198 ± 43 |
| | 4 | 22 | 227 ± 36 |
| | 5 | 18 | 196 ± 26 |
| | 6 | 16 | 181 ± 28 |
| Horizontal-direction | 1 | 23 | 225 ± 13 |
| | 2 | 21 | 234 ± 29 |
| | 3 | 20 | 226 ± 25 |
| | 4 | 17 | 214 ± 19 |
| | 5 | 22 | 185 ± 26 |
| | 6 | 14 | 175 ± 47 |

*$n$ = 5.

which agreed well with the transfer ratio of the injection molding, especially the depth of the nanoperiodic structure. For the nanoperiodic structure that was applied in the uniaxial direction, the apparent contact angles did not decrease with respect to the direction, whereas the circularity tolerances changed by 5% for the different directions. As a result, the apparent contact angle increased by 20.4°, from 77.2° to 97.6°, which is equivalent to an improvement of 26%. The equilibrium contact angle on the flat plate (77.2°) was <90° and the apparent contact angle was increased by forming a periodic structure. Under static evaluation conditions using a 1 μL water drop, it was considered that a laser-induced nanoperiodic structure with a 780 nm pitch follows the Cassie regime.[25]

Finally, the hydrophobicity was evaluated throughout the six-month duration test by measuring the sliding angle and the CAH. AES was used as the test material because its 'weatherability' is superior to other plastic resins. The sliding angle was maintained between 20° and 38.3° during the duration test, which was lower than that of flat plate at 42.7°. Throughout the duration test, the depth decreased to 40% of the initial value, which was induced by erosion of the nanoperiodic structure on the surface. According to these observations, it was considered that a depth of about 175–181 nm was sufficient to maintain the sliding angle.

On the other hand, the CAH did not differ with or without the nanoperiodic structure on the surfaces. The CAH directly characterizes resistance to mobility; low values confirm a lack of pinning, consistent with a nearly defect-free surface.[26,27] Then force needed to start a drop moving over a solid surface (moving force) is proportional to ($\cos\theta_R - \cos\theta_A$) in Furmidges equation.[24,28] Both the CAH and the moving force did not differ with and without the presence of a nanoperiodic structure. One reason for this phenomenon was considered to be that surface dirt gradually increased with time, which can be estimated from the color difference. Additionally, there is a possibility that a laser-induced nanoperiodic structure with a 780-nm pitch does not perfectly follow the Cassie regime under these evaluation conditions using a 30 μL water drop.

In summary, the apparent contact angle characteristics did not agree with the sliding angle and the CAH in an exterior environmental exposure duration test. Therefore, the hydrophobicity should be evaluated using the sliding angle and the CAH. It was

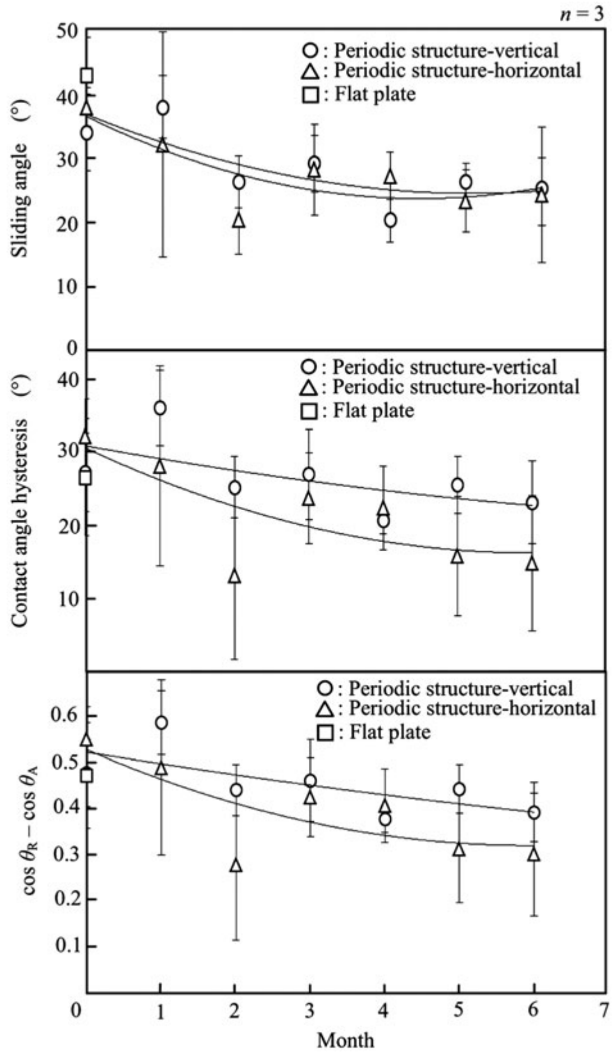


Figure 4. Time-course changes of the sliding angle and the CAH in an exterior environmental exposed durability test for 6 months ($\theta_A$: advancing angle, $\theta_R$: receding angle, error bar: SD).

revealed that the plastic plate was well drained and the characteristics were maintained at a higher level during the first several months by forming the nanoperiodic structure. It could be useful to use the photocatalytic materials such as $TiO_2$ to cover the initial characteristic of them [29] since the photoinduced redox reaction on a photocatalyst fluctuates with the level of sunlight, which changes with time.

## 5. Conclusions

Our results indicated that a processing method for manufacturing wide-area nanoperiodic structures on plastic plates could be established using a femtosecond laser and an injection molding technique. It was revealed that the apparent contact angle agreed well with the transfer ratio of the depth of the nanoperiodic structure. When the nanoperiodic structure was applied in the uniaxial direction, the apparent contact angles did not decrease with respect to the direction of the ridges. It was also revealed that the plastic plate was well drained and the characteristics were maintained at a higher level during the first several months by forming the nanoperiodic structure.

## Funding

This research was supported in part by from the Japan Society for the Promotion of Science from [grant number 25350517], Proposal for Fluid Control Mechanism based on Wettability and Establishment of Quantitative and Automated- biosensor (P.I.-M. Yamaguchi), Japan.

## References

[1] Rosado BHP, Holder CD. The significance of leaf water repellency in ecohydrological research: a review. Ecohydrology. 2013;6:150–161.
[2] Fürstner R, Barthlott W, Neinhuis C, Walzel P. Wetting and self-cleaning properties of artificial superhydrophobic surfaces. Langmuir. 2005;21:956–961.
[3] Solga A, Cerman Z, Striffler BF, Spaeth M, Barthlott W. The dream of staying clean: lotus and biomimetic surfaces. Bioinspir. Biomim. 2007;2:S126–S134.
[4] Nosonovsky M, Bhushan B. Green tribology. Lotus versus rose: biomimetic surface effects. Heidelberg: Springer-Verlag; 2008. p. 25–40.
[5] Gao L, McCarthy TJ, Zhang X. Wetting and superhydrophobicity. Langmuir. 2009;25: 14100–14104.
[6] Dodiuk H, Kenig S, Dotan A. Do self-cleaning surfaces repel ice? J. Adhes. Sci. Technol. 2012;26:701–714.
[7] Ueda E, Levkin PA. Emerging applications of superhydrophilic–superhydrophobic micropatterns. Adv. Mater. 2013;25:1234–1247.
[8] Wang B-B, Feng J-T, Zhao Y-P, Yu TX. Fabrication of novel superhydrophobic surfaces and water droplet bouncing behavior – Part 1: stable ZnO–PDMS superhydrophobic surface with low hysteresis constructed using ZnO nanoparticles. J. Adhes. Sci. Technol. 2010;24:2693–2705.
[9] Wang B-B, Feng J-T, Zhao Y-P, Yu TX. Fabrication of novel superhydrophobic surfaces and droplet bouncing behavior – Part 2: water droplet impact experiment on superhydrophobic surfaces constructed using ZnO nanoparticles. J. Adhesion Sci. Technol. 2010;25:93–108.
[10] Yamaguchi M, Sasaki Y, Sasaki M, Hirose K. Improvement of water repellency of biomass plastic molding by fractal micro-structure on mold surface. Trans. J. Soc. Mech. Eng. Ser.B. 2011;77:1127–1129 [in Japanese].
[11] Birnbaum R. Semiconductor surface damage produced by ruby lasers. J. Appl. Phys. 1965;36:3688–3689.
[12] Bolle M, Lazare S. Submicron periodic structures produced on polymer surfaces with polarized excimer laser ultraviolet radiation. Appl. Phys. Lett. 1992;60:674–676.
[13] Bonch-Bruevich AM, Libenson MN, Markin VS, Trubaev V. Surface electromagnetic waves in optics. Opt. Eng. 1992;31:718–730.
[14] Emmony DC, Howson RP, Willis LJ. Laser mirror damage in germanium at 10.6 μm. Appl. Phys. Lett. 1973;23:598–600.
[15] Kietzig A-M, Mirvakili MN, Kamal S, Englezos P, Hatzikiriakos SG. Laser-patterned superhydrophobic pure metallic substrates: cassie to wenzel wetting transitions. J. Adhes. Sci. Technol. 2011;25:2789–2809.
[16] Yamaguchi M, Kaneko Y, Sasaki M. Fabrication of nano-periodic structure on plastic film for water repellent using femtosecond laser. Trans. Control Mech. Syst. 2012;1:306–311.
[17] ISO 1133-1. Plastics – determination of the melt mass-flow rate (MFR) and the melt volume-flow rate (MVR) of thermoplastics. Geneva: ISO; 2011. p. 1–24.
[18] ISO 178. Plastics – determination of flexural properties. Geneva: ISO; 2010. p. 1–19.
[19] ISO 527-2. Plastics – determination of tensile properties – Part 2: test conditions for moulding and extrusion plastics. Geneva: ISO; 2012. p. 1–24.

[20] Ruiz-Cabello FJM, Rodríguez-Valverde MA, Cabrerizo-Vílchez MA. Equilibrium contact angle or the most-stable contact angle? Adv. Colloid. Interface. Sci. 2014;206:320–327.
[21] Strobel M, Lyons CS. An essay on contact angle measurements. Plasma Processes Polym. 2011;8:8–13.
[22] Románszki L, Mohos M, Telegdi J, Keresztes Z, Nyikos L. A comparison of contact angle measurement results obtained on bare, treated, and coated alloy samples by both dynamic sessile drop and Wilhelmy method. Period. Polytech. Chem. Eng. 2014;58:53–59.
[23] Krasovitski B, Marmur A. Drops down the hill: theoretical study of limiting contact angles and the hysteresis range on a tilted plate. Langmuir. 2005;21:3881–3885.
[24] Rios PF, Dodiuk H, Kenig S, McCarthy S, Dotan A. The effect of polymer surface on the wetting and adhesion of liquid systems. J. Adhes. Sci. Technol. 2007;21:227–241.
[25] Yamaguchi M, Suzuki S, Sasaki S, Chiba T, Itoh N, Hoga M. Fabrication of nano-periodic structures and modification of the Wenzel model to estimate contact angle. Sens. Actuators, A. 2014;212:87–92.
[26] Delmas M, Monthioux M, Ondarcuhu T. Contact angle hysteresis at the nanometer scale. Phys. Rev. Lett. 2011;106:136102-1–136102-4.
[27] Wong T-S, Kang SH, Tang SKY, Smythe EJ, Hatton BD, Grinthal A, Aizenberg J. Bioinspired self-repairing slippery surfaces with pressure-stable omniphobicity. Nature. 2011;477:443–447.
[28] Chen W, Fadeev AY, Hsieh MC, Öner D, Youngblood J, McCarthy TJ. Ultrahydrophobic and ultralyophobic surfaces: some comments and examples. Langmuir. 1999;15:3395–3399.
[29] Hashimoto K, Irie H, Fujishima A. $TiO_2$ photocatalysis: a historical overview and future prospects. Jpn. J. Appl. Phys. 2005;44:8269–8285.